Journal of Southeast University (English Edition) Vol. 38, No. 1, pp. 27 – 35 Mar. 2022 ISSN 1003—7985

Finite rate of innovation sparse sampling for a binary frequency-coded ultrasonic signal

Song Shoupeng Chen Yiqian Xu Baowen Qiu Yue

(School of Mechanical Engineering, Jiangsu University, Zhenjiang 212013, China)

Abstract: To achieve sparse sampling on a coded ultrasonic signal, the finite rate of innovation (FRI) sparse sampling technique is proposed on a binary frequency-coded (BFC) ultrasonic signal. A framework of FRI-based sparse sampling for an ultrasonic signal pulse is presented. Differences between the pulse and the coded ultrasonic signal are analyzed, and a response mathematical model of the coded ultrasonic signal is established. A time-domain transform algorithm, called the high-order moment method, is applied to obtain a pulse stream signal to assist BFC ultrasonic signal sparse sampling. A sampling of the output signal with a uniform interval is then performed after modulating the pulse stream signal by a sampling kernel. FRI-based sparse sampling is performed using a self-made circuit on an aluminum alloy sample. Experimental results show that the sampling rate reduces to 0.5 MHz, which is at least 12.8 MHz in the Nyquist sampling mode. The echo peak amplitude and the time of flight are estimated from the sparse sampling data with maximum errors of 9.324% and 0.031%, respectively. This research can provide a theoretical basis and practical application reference for reducing the sampling rate and data volume in coded ultrasonic testing.

Key words: coded ultrasonic signal; finite rate of innovation; high-order moment; sparse sampling; circuit implementation

DOI: 10.3969/j.issn.1003 – 7985.2022.01.005

Ultrasonic waves are generally generated using a single-pulse excitation technique with existing ultrasonic testing equipment, and their peak acoustic power is directly determined using the pulse amplitude. Even if the emission voltage increases to its upper limit, the average acoustic power is low, which results in a low signal-to-noise ratio (SNR) of the echo signal. A coded excitation method can effectively solve this problem. The duration of a continuous coding sequence is longer than that of a single pulse in the time domain. Thus, the average sound power and echo SNR are effectively improved without increasing the emission voltage[1-2]. Most common ultrasonic coded forms include the M-sequence pseudo-random coding[3], Huffman sequence[4], Barker code[5], Golay code[6], and linear and nonlinear frequency modulation[7].

Unlike the traditional Nyquist sampling, the finite rate of innovation (FRI) sampling theory was first proposed by Vetterli et al.[8] in 2002. However, this theory is just for FRI signals, which can be represented by finite degrees of freedom, and the degree of freedom per unit time is called the rate of innovation (ROI). According to the FRI sampling theory, sparse sampling data are obtained by uniform space sampling of the signal that is processed using a properly designed sampling kernel whose sampling frequency is much lower than that of a traditional sampling technique. Using this method, the A/D sampling rate can be greatly reduced and the key parameters of a signal, such as the echo amplitude and time of flight, can be accurately estimated from the sparse sampling data. Therefore, the sampling technique can be applied to cases that require a great reduction of a large amount of sampling data[9]. Until now, the FRI sampling theory has been applied to fields of super-wideband communication, GPS, radar, medical ultrasonic imaging, and industrial ultrasonic testing[10-12].

The FRI sampling theory was originally proposed for four typical FRI signals, namely the Dirac stream signal, differential Dirac stream signal, non-uniform spline, and piecewise polynomial signal[8]. In subsequent research, the piecewise sinusoidal signal[13] and a pulse signal of known shape[14] were incorporated into the types of signals that can be FRI-sampled.

The ultrasonic signal in the form of a single-pulse excitation can be transformed into a pulse stream signal to satisfy FRI sampling requirements. Tur et al.[15] introduced the FRI sampling method to the medical ultrasonic imaging field in 2011. Peng[16] first applied this method to the field of pipeline flaw ultrasonic array testing in 2015. Since the coded ultrasonic signal does not satisfy FRI sampling requirements, it cannot be directly FRI-sampled. To solve this problem, this paper proposes a novel signal transformation technique to obtain a pulse stream of the coded ultrasonic signal to satisfy FRI sparse sampling conditions. Meanwhile, a circuit has been designed to perform the proposed method.

Received 2021-09-10, **Revised** 2021-12-02.

Biography: Song Shoupeng (1967—), male, doctor, professor, songshoupeng@126.com.

Foundation item: The National Natural Science Foundation of China (No. 51375217).

Citation: Song Shoupeng, Chen Yiqian, Xu Baowen, et al. Finite rate of innovation sparse sampling for a binary frequency-coded ultrasonic signal[J]. Journal of Southeast University (English Edition), 2022, 38(1): 27 – 35. DOI: 10.3969/j.issn.1003 – 7985.2022.01.005.

1 FRI Sparse Sampling of a Pulse-Excited Ultrasonic Signal

The mathematical model of a pulse-excited ultrasonic signal can be expressed as a Gaussian modulated signal and expressed as[16]

$$s(t) = \sum_{l=1}^{L} \beta_l \, \mathrm{e}^{-(t-t_l)^2/\alpha_l^2} \cos(2\pi f_0 (t - t_l) + \phi_l) \quad (1)$$

where L is the number of echoes in one signal; β_l is the amplitude coefficient of the echo; α_l is the pulse width factor of the echo; t_l is the time of flight of the echo; f_0 is the center frequency of the ultrasonic transducer; and ϕ_l is the initial phase.

The Gaussian pulse envelope $g(t)$ can be extracted as

$$g(t) = \sum_{l=1}^{L} \beta_l \, \mathrm{e}^{-(t-t_l)^2/\alpha_l^2} \quad (2)$$

We define $g(t)$ as the ultrasonic pulse stream, which can be determined by finite degrees of freedom $\{\beta_l, t_l\}_{l=1}^{L}$ if the pulse width factor α_l of the Gaussian envelope is prior known. Therefore, $g(t)$ can be sparse-sampled using the FRI-based method.

Suppose the time duration of the ultrasonic echo signal is τ, the ROI of the pulse stream can then be calculated as follows[8]:

$$\mathrm{ROI} = \frac{2L}{\tau} \quad (3)$$

Fig. 1 shows the FRI sparse sampling framework of a pulse-excited ultrasonic signal. First, the reflected ultrasonic signal $s(t)$ from the test object is transformed into an ultrasonic pulse stream signal $g(t)$. Then, $g(t)$ is processed using the FRI sampling kernel to obtain the output signal $y(t)$. The sparse sampling data $y[n]$ are then obtained by sampling $y(t)$ with uniform intervals at a low sampling rate, which is not lower than ROI. Finally, the estimated signal $\hat{g}(t)$ is obtained by parameter estimation and estimation algorithms, such as the annihilating filter method[8], matrix pencil method[17], and singular value decomposition method[18].

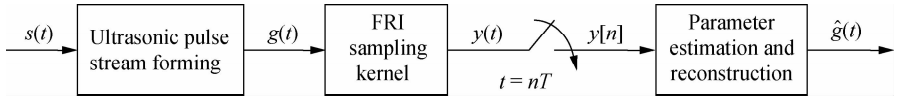

Fig. 1 Framework of FRI sparse sampling for a pulse-excited ultrasonic signal

2 FRI Sparse Sampling Framework of a Coded Ultrasonic Signal

2.1 Mathematical model of a binary frequency-coded ultrasonic signal

A coded ultrasonic signal is applied to improve the average sound power and echo SNR. This is more convenient for frequency selection and debugging. Therefore, it was selected as the coding increasing the emission voltage. Moreover, a frequency coding form can impart abundant frequency information to an ultrasonic detection signal, which can improve the frequency sensitivity of the ultrasonic detection signal to different sizes and types of defects, thereby improving the defect detection rate.

The binary frequency-coded (BFC) signal $c(t)$ is expressed as

$$\begin{aligned} c(t) = & \sum_{k_1=1}^{K} \left[\frac{2}{\pi} b_{k_1} E G(-k_1 \tau_1) \cdot \right. \\ & \left. \sum_{m=1}^{M} \frac{1}{m} \sin^2\left(\frac{m\pi}{2}\right) \sin(m\omega_1 t) \right] + \\ & \sum_{k_2=1}^{K} \left[\frac{2}{\pi} b_{k_2} E G(-k_2 \tau_2) \cdot \right. \\ & \left. \sum_{m=1}^{M} \frac{1}{m} \sin^2\left(\frac{m\pi}{2}\right) \sin(m\omega_2 t) \right] \end{aligned} \quad (4)$$

where K is the total length of the coded excitation signal, $K \in \mathbf{Z}^+$; $G(t - k\tau)$ is a rectangular window function with length τ; $b_{k_i} = \begin{cases} 0 \\ 1 \end{cases}$, $i = 1, 2$, and $b_{k_1} b_{k_2} = 0$, $\omega_i (i = 1, 2)$ is the fundamental frequency of a trigonometric function; M is the harmonic order, $M \in \mathbf{Z}^+$; and E is a constant.

Let us assume that the response function of an ultrasonic transducer is as follows[12]:

$$h(t) = \beta \, \mathrm{e}^{-ct^2} \cos(\omega_0 t + \phi) \quad (5)$$

where β is the amplitude coefficient; $c = 1/\gamma^2$; γ is the pulse width coefficient; ω_0 is the center frequency of the ultrasonic transducer; and ϕ is the initial phase.

Then, the response of the coded signal $c(t)$ through the ultrasonic transducer is as follows:

$$\begin{aligned} x(t) = & F^{-1}[X(\omega)] = F^{-1}[C(\omega) H(\omega)] = \\ & E\beta \, \mathrm{e}^{-ct^2} \left[\sum_{k_1=1}^{K} b_{k_1} G(t - k_1 \tau_1) \cos(\omega_1 t + \phi) + \right. \\ & \left. \sum_{k_2=1}^{K} b_{k_2} G(t - k_2 \tau_2) \cos(\omega_2 t + \phi) \right] \end{aligned} \quad (6)$$

where $F^{-1}[\cdot]$ denotes the inverse Fourier transform; $X(\omega)$, $C(\omega)$, and $H(\omega)$ are the Fourier transforms of $x(t)$, $c(t)$, and $h(t)$, respectively.

$$\begin{aligned} C(\omega) = & \sum_{k_1=1}^{K} \frac{\tau_1 \, b_{k_1} E}{\pi} Sa\left[\frac{(\omega - \omega_1)\tau_1}{2}\right] + \\ & \sum_{k_2=1}^{K} \frac{\tau_2 \, b_{k_2} E}{\pi} Sa\left[\frac{(\omega - \omega_2)\tau_2}{2}\right] \end{aligned} \quad (7)$$

$$H(\omega) = \frac{1}{2}\sqrt{\pi}\beta\gamma\, \mathrm{e}^{-((\omega-\omega_0)\gamma/2)^2} \tag{8}$$

Figs. 2(a) and (b) illustrate four-bit BFC excitation signals. The frequencies of low- and high-frequency code elements are 3.2 and 6.4 MHz, respectively. Figs. 2(c) and (d) illustrate the coded ultrasonic echo signals reflected from the flat bottom aluminum alloy sample. The center frequency of the ultrasonic transducer is 5 MHz with a bandwidth of 4 MHz. Fig. 2 indicates that this type of signal has a longer oscillation and a more complicated waveform than a pulse-excited ultrasonic signal.

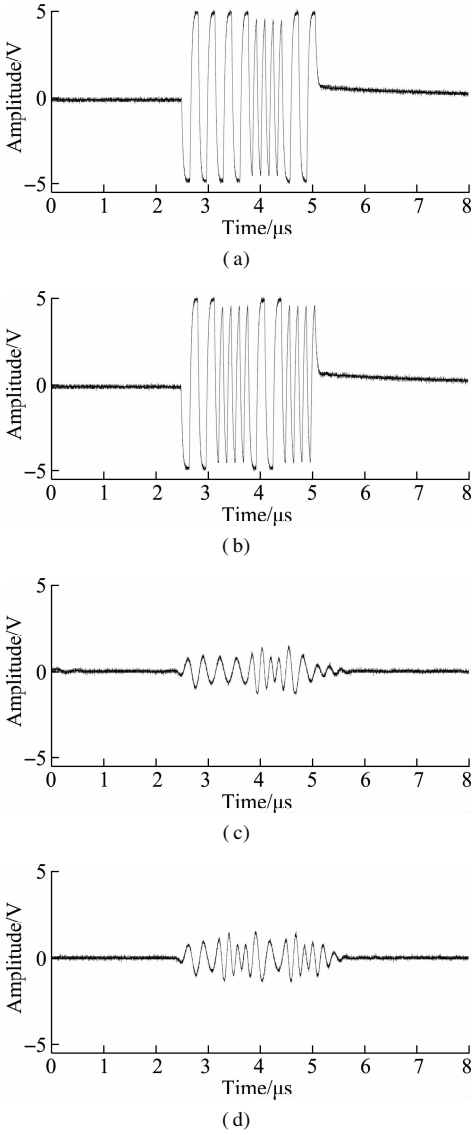

Fig. 2 Binary frequency-coded excitation signals and ultrasonic echo signals. (a) Coded excitation signal 0010; (b) Coded excitation signal 0101; (c) Coded ultrasonic echo signal 0010; (d) Coded ultrasonic echo signal 0101

The coded ultrasonic echo is more complex than the pulse ultrasonic pulse in a waveform, which needs more parameters to determine it. Thus, it does not satisfy the FRI-based sparse sampling conditions for ultrasonic pulse echo; that is to say it cannot be determined by two degrees of freedom $\{\beta_l, t_l\}_{l=1}^{L}$. Therefore, it cannot be FRI-based sparse sampling directly. Considering that the primary information of the coded ultrasonic echo is also the amplitude coefficient and the time of flight, if we can find a way to express the coded ultrasonic echo using these two parameters, the FRI-based sparse sampling method would then be applied to it.

2.2 High-order moment of coded ultrasonic and FRI sampling

Let us assume that the coded echo signal $x_r(t)$ reflected from the bottom of the test sample is as follows:

$$x_r(t) = \beta' x(t) \tag{9}$$

The pulse compression signal $x_m(t_0)$ by extracting the second-order moment of the coded echo signal can then be obtained as follows:

$$\begin{aligned} x_m(t_0) &= \lim_{T\to\infty}\left[\frac{1}{T}\int_{-\frac{T}{2}}^{\frac{T}{2}} x_r(t)\, x_r(t-t_0)\,\mathrm{d}t\right] = \\ &(E\beta\beta')^2\left[\cos(\omega_1 t_0)\sum_{k_1=1}^{K} b_{k_1} G(t-k_1\tau_1)\cdot\right. \\ &G(t-t_0\ k_1\tau_1) + \cos(\omega_2 t_0)\sum_{k_2=1}^{K} b_{k_2} G(t- \\ &\left. k_2\tau_2)\, G(t-t_0-k_2\tau_2)\right]\frac{\pi}{2c} \end{aligned} \tag{10}$$

where β' is the reflection attenuation coefficient and t_0 is the amount of delay processing for one of the echo signals.

To improve the SNR and time resolution of the coded ultrasonic signal, a pulse compression[19] technique is generally performed on its echo signal using a matching filtering method[20–22], which is a second-order moment method.

According to the Wiener-Khintchine theorem[23], the autocorrelation function of a coded ultrasonic echo signal is the inverse Fourier transform of its power spectrum function, and the peak point of the matched filter output signal appears at $t = t_0$, with its amplitude equal to the energy value $P = \frac{(E\beta\beta')^2}{2}\frac{\pi}{c}$ of the coded ultrasonic echo signal $x_r(t)$. Clearly, the peak point amplitude is independent of the waveform of $x_r(t)$, which is only related to its energy value P; i.e., the matched filter can concentrate the energy of a coded ultrasonic echo signal on the peak of its output signal, which can improve the average sound power of the signal.

Figs. 3(a) and (b) present the second-order moment waveforms of Figs. 2(c) and (d), respectively. The sidelobe level of the signal that was compressed using the matched filter is still high, because it is difficult to obtain the signal ROI and the accurate parameters of the coded ultrasonic echo signal. To suppress the sidelobes and

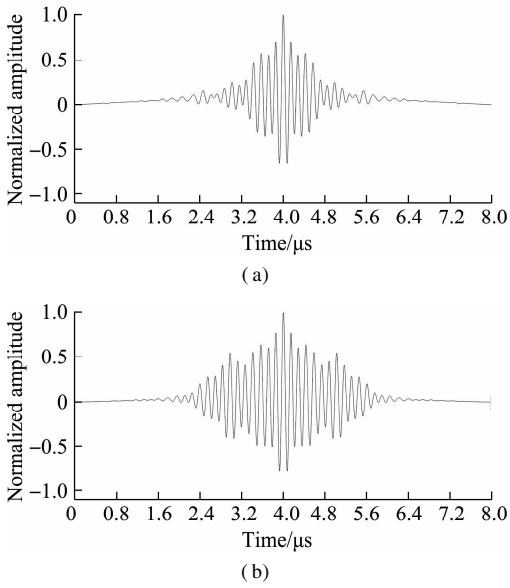

Fig. 3 Second-order moment of the coded ultrasonic signal. (a) Coded ultrasonic echo signal 0010; (b) Coded ultrasonic echo signal 0101

highlight the mainlobe, a mismatched filter is constructed by adding a window function in the matched filter[24-25]; however, this method increases the mainlobe width and decreases the mainlobe amplitude.

To overcome the shortcomings of the second-order moment method, a high-order moment $x_{\mathrm{H}}(t_0)$ of coded ultrasonic echo signals is introduced, which can be expressed as

$$x_{\mathrm{H}}(t_0) = [x_m(t_0)]^{2n} \qquad n \in \mathbf{Z}^+ \tag{11}$$

If the mainlobe amplitude $P_{\mathrm{H}} \geqslant 1$ and the sidelobe amplitude $P_{\mathrm{L}} < 1$, the mainlobe amplitude of a high-order moment $x_{\mathrm{H}}(t_0)$ is then maintained or increased and each sidelobe is attenuated. The higher the order $2n$, the greater the attenuation. If both the mainlobe and sidelobe amplitudes $P_{\mathrm{H}} < 1$ and $P_{\mathrm{L}} < 1$, the amplitudes of the mainlobe and sidelobe of the high-order moment $x_{\mathrm{H}}(t_0)$ are attenuated. As the mainlobe concentrates the main energy of the second-order moment, assuming that the minimum ratio of mainlobe to sidelobe amplitudes is $\Delta P = P_{\mathrm{H}}/P_{\mathrm{L}}$, the attenuation gradient of the sidelobe is then larger than that of the mainlobe. This has the same effect of enhancing the mainlobe and suppressing the sidelobe.

Fig. 4 shows the high-order moment of the BFC ultrasonic echo signal 0010. The higher the order, the larger the ratio ΔP of the mainlobe and sidelobe amplitudes, i. e., the mainlobe is being enhanced. Clearly, the high-order moment signal $x_{\mathrm{H}}(t_0)$ can be characterized by using two finite information degrees of freedom, namely the peak amplitude and the peak arrival time of the mainlobe, $\{P_{\mathrm{H}l}, t_{\mathrm{H}l}\}_{l=1}^{L}$, which correspond to the echo signal amplitude and the time of flight, respectively. Meanwhile, the processed signal satisfies the characteristics of an FRI signal, so it can be sparse-sampled based on FRI.

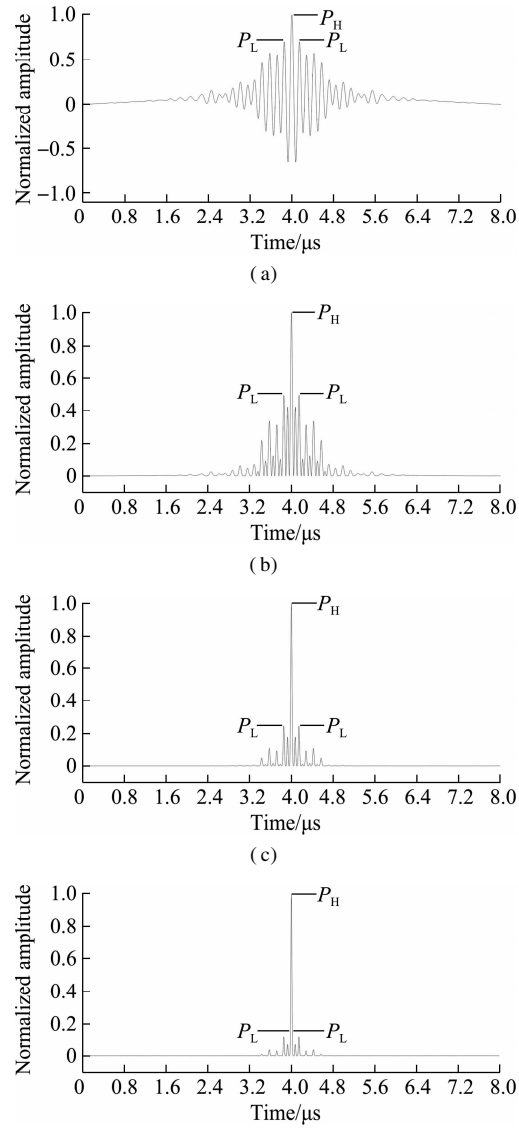

Fig. 4 High-order moment of a coded ultrasonic signal. (a) Second-order moment; (b) Fourth-order moment; (c) Eighth-order moment; (d) Twelfth-order moment

The amplitude ratio ΔP increases greatly for higher order moments $x_{\mathrm{H}}(t_0)$. Therefore, the SNR of the coded ultrasonic echo signal will be greatly improved with higher order moment processing. The amplitude $P_{\mathrm{H}l}$ and time of flight $t_{\mathrm{H}l}$ can represent the signal $x_{\mathrm{H}}(t_0)$. According to the high-order moment conversion process, these two parameters $\{P_{\mathrm{H}l}, t_{\mathrm{H}l}\}_{l=1}^{L}$ of the high-order moment signal $x_{\mathrm{H}}(t_0)$ can be estimated from the $\{P_l, t_l\}_{l=1}^{L}$ of the coded ultrasonic echo signal $x_{\mathrm{r}}(t)$ as follows:

$$\left.\begin{aligned} P_{\mathrm{H}l} &= P_l^{2n} = \left[\frac{(E\beta\beta')^2}{2}\frac{\pi}{c}\right]^{2n} \\ t_{\mathrm{H}l} &= t_l + t_0 = \frac{t_{sl} + t_{el}}{2} + t_0 \end{aligned}\right\} \tag{12}$$

where $2n$ is the order of the high-order moment; t_{sl} is the oscillation start time of the coded ultrasonic echo signal; t_{el} is the oscillation end time of the coded ultra-

sonic echo signal; and t_0 is the time delay of the processing system.

2.3 FRI sampling method of the coded ultrasonic echo signal

The FRI sampling process of the coded ultrasonic echo signal can be summarized as follows:

1) Generating the coded excitation signal $c(t)$ according to coding rules;

2) Driving the ultrasonic transducer by power amplification to generate the coded ultrasonic detection signal $x(t)$;

3) Obtaining the reflected echo $x_r(t)$ from the test object;

4) Obtaining the high-order moment signal $x_H(t_0)$ from the echo signal $x_r(t)$;

5) Performing FRI sparse sampling on $x_H(t_0)$ to obtain sparse sampling data $y[n]$;

6) Estimating the peak amplitude and time of flight $\{P_{Hl}, t_{Hl}\}_{l=1}^{L}$ of $x_H(t_0)$ using the annihilating filter method;

7) Estimating the parameters of the amplitude and time of flight $\{P_l, t_l\}_{l=1}^{L}$ of the coded ultrasonic echo signal.

Fig. 5 presents the framework of FRI sparse sampling for the coded ultrasonic echo signal.

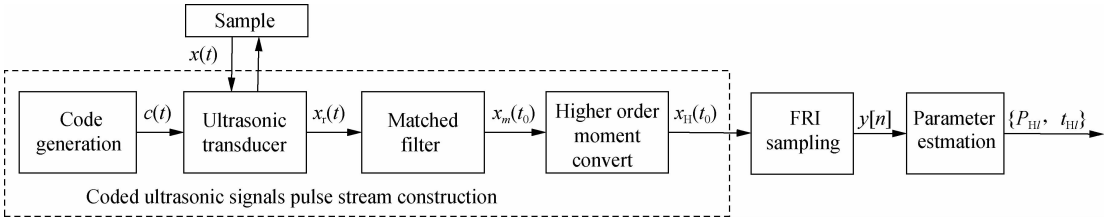

Fig. 5 FRI sparse sampling framework of the coded ultrasonic signal

3 Circuit Design of the Sparse Sampling Framework

To verify the effectiveness and performance of the proposed method, a circuit has been designed. Fig. 6 shows the circuit block diagram.

The circuit includes a code generation module, echo-receiving module, matched filter module, high-order moment convert module, and FRI sampling kernel circuit model. The coded excitation signal is generated using the code generation module for exciting the ultrasonic transducer, and the coded ultrasonic echo signal is pre-amplified and bandpass-denoised using the echo-receiving module. The second-order moment of the echo signal is then extracted using the matched filter module. The high-order moment of the echo signal is further transformed using the high-order moment convert module to generate the ultrasonic pulse stream with its output signal amplified again by a post-amplifier. Finally, the FRI sampling kernel is applied for subsequent data sampling with a uniform interval at a low sampling rate.

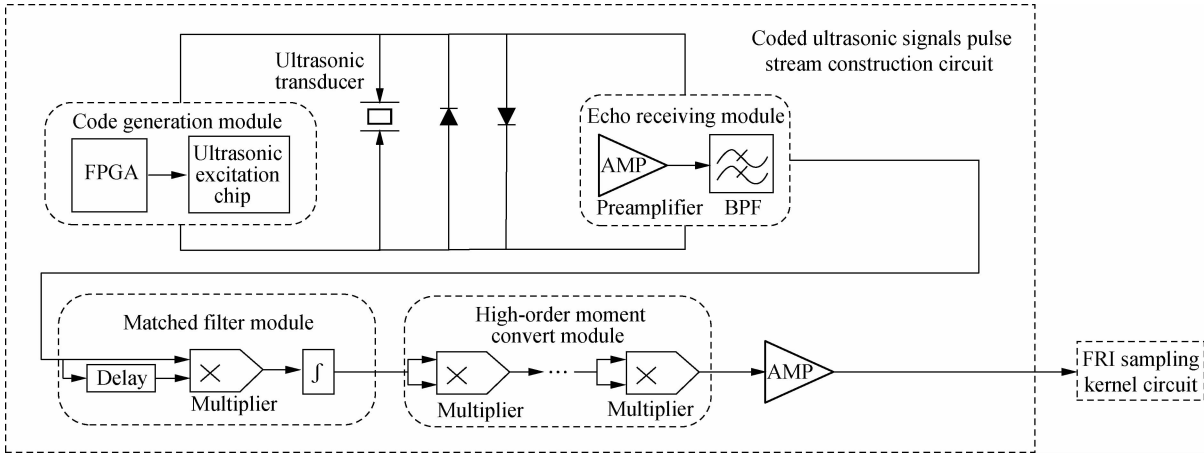

Fig. 6 Circuit block diagram of FRI sparse sampling of the coded ultrasonic signal

Code generation module: An FPGA is used as the control chip to generate a BFC signal $c(t)$; the frequency of the low-frequency code element "0" is set to 3.2 MHz, the frequency of the high-frequency code element "1" is set to 6.4 MHz, and the code length is set to 4 bit; i. e., there are 2^4 coding forms from 0000 to 1111. The ultrasonic excitation chip is used to amplify the BFC signal into a high-energy-coded excitation signal with an amplitude of ± 60 V, exciting the ultrasonic transducer to generate a coded ultrasonic signal.

Echo-receiving module: The preamplifier circuit consists of the operational amplifier, which is used for impedance matching and preamplification of the coded ultrasonic echo signal $x_r(t)$. Preamplification aims to ad-

just the amplitude of the coded ultrasonic signal in a proper range to fit subsequent signal processing. The second-order Butterworth bandpass filter circuit consists of the operational amplifier. The central frequency of the passband is set to 5 MHz, the bandwidth is set to 4 MHz with the passband attenuation set to −3 dB, and the stopband attenuation is set to −40 dB.

Matched filter module: This module divides the echo signal into two signals and delays one of them. The delay circuit consists of a second-order Bessel lowpass filter implemented with the passband cutoff frequency set to 10 MHz, passband attenuation set to −3 dB, and the stopband attenuation set to −40 dB. Because of the large group delay of the Bessel filter, the echo signal can be delayed by hundreds of nanoseconds. The two signals are connected to the four-quadrant multiplier, and the output of the multiplier is connected to an implemented integral circuit. The second-order moment of the coded ultrasonic signal $x_m(t_0)$ is then obtained.

High-order moment conversion module: The second-order moment $x_m(t)$ is connected to the four-quadrant multiplier for multiplication, and the result of the multiplication is its high-order moment. More multipliers are required for higher orders. The high-order moment of a coded ultrasonic echo signal is finally constructed into an ultrasonic pulse stream signal $x_H(t_0)$ by gain adjustment.

Part of the FRI sampling kernel hardware circuit is implemented using a Chebyshev lowpass filter to form a Fourier series coefficient screening circuit for approximation, which then directly samples it using the FRI sparse sampling circuit. According to the characteristics of the input signal and results of the subsequent parameter estimation algorithm, the conditions for a sampling kernel to be satisfied are determined. After the input signal passes through the FRI sampling kernel circuit, sparse sampling can be performed on it at its ROI, and the major parameters can be estimated using the sparse-sampled data through the parameter estimation algorithm.

4 Experimental Results and Analysis

An experimental platform was established to verify the effectiveness of the proposed method for pulse stream forming and FRI sampling, as shown in Fig. 7. In the experiments, a 4-bit BFC ultrasonic detection signal was adopted, and a test signal was applied to an aluminum alloy sample to obtain the flat bottom echo. The high-order moment of the coded ultrasonic echo signal was then obtained using the pulse stream construction circuit. The ultrasonic pulse stream signal was processed using the FRI sampling kernel circuit to obtain the FRI sampling kernel output signal. Finally, the signal was sparse-sampled at a low sampling rate with uniform intervals to obtain the sparse sampling data.

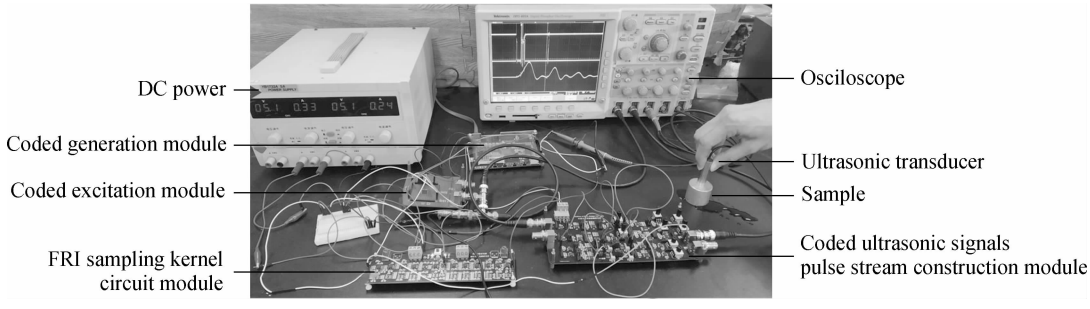

Fig. 7 Experimental platform

In the experiment, a T/R immersion normal ultrasonic transducer with a central frequency of 5 MHz and bandwidth of 4 MHz was used. Water was used as a coupling medium. The thickness of the aluminum alloy sample was 20 mm, the frequency of the low-frequency code element "0" was set to 3.2 MHz, the frequency of the high-frequency code element "1" was set to 6.4 MHz, and the code length was set to 4 bit.

Using the coded ultrasonic signal 0010 and 0101 as examples, Figs. 8 (a) and (b) show the initial pulse and bottom echo of the coded ultrasonic signals 0010 and 0101. Figs. 8 (c) and (d) show the pulse stream, FRI sampling kernel output, and FRI sampling points of the two coded signals, respectively. Figs. 8 (e) and (f) present a comparison of the pulse stream and the estimated signal with the parameters estimated using the FRI sparse sampling data, respectively. According to the Nyquist-Shannon sampling theorem, the A/D sampling rate of the coded ultrasonic detection signal needs to be no less than 12.8 MHz. In the experiment, the number of pulse echoes is $L_1 = 2$, the signal duration is $\tau_1 \approx 8\ \mu s$, and the local maximum innovation rate of the ultrasonic pulse stream is $\mathrm{ROI}_1 = 2L_1/\tau_1 \approx 0.5 \times 10^6$, that is only 4% of the conventional sampling frequency. The high-order moment in this experiment was the twelfth one. Clearly, the mainlobe amplitude of the coded ultrasonic echo signal was greatly increased and the sidelobe amplitude was greatly attenuated. An annihilating filter algorithm was used to estimate the signal peak amplitude and time of flight of the pulse stream using the sparse-sampled data.

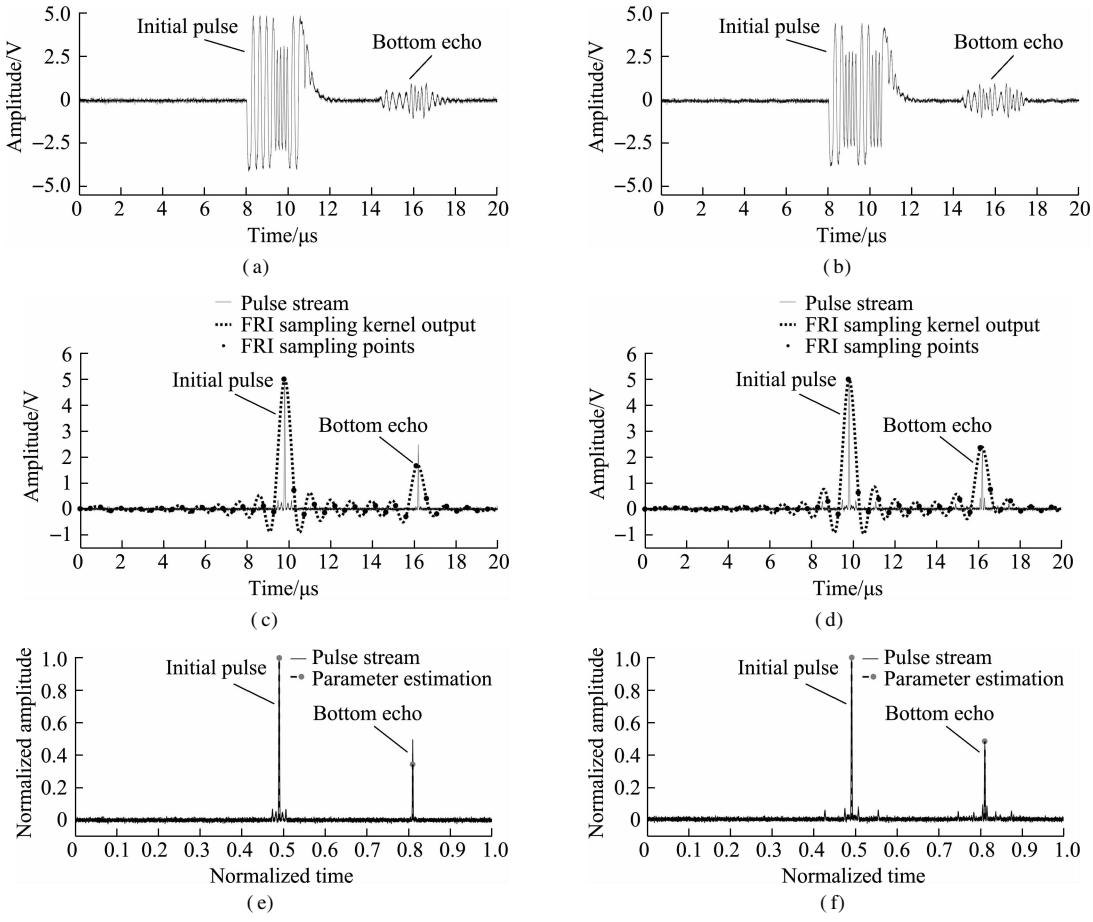

Fig. 8 Experimental results of two coded ultrasonic signals 0010 and 0101. (a) Initial pulse and bottom echo of the coded ultrasonic signal 0010; (b) Initial pulse and bottom echo of coded ultrasonic signal 0101; (c) Pulse stream and sampling kernel output of the coded ultrasonic signal 0010; (d) Pulse stream and sampling kernel output of the coded ultrasonic signal 0101; (e) Estimated result of the coded ultrasonic signal 0010; (f) Estimated result of the coded ultrasonic signal 0101

Fig. 9 shows the amplitude and time parameter estimation errors of the 2^4 binary frequency coding forms. The high-order moment is twelfth. P_{Hl} and t_{Hl} are actual values; P'_{Hl} and t'_{Hl} are estimated values. Both of them were obtained by averaging 10 data samples. The formula of the estimation error is expressed as

$$\Delta P_{Hl} = \frac{|P'_{Hl} - P_{Hl}|}{P_{Hl}} \times 100\%$$

$$\Delta t_{Hl} = \frac{|t'_{Hl} - t_{Hl}|}{t_{Hl}} \times 100\%$$

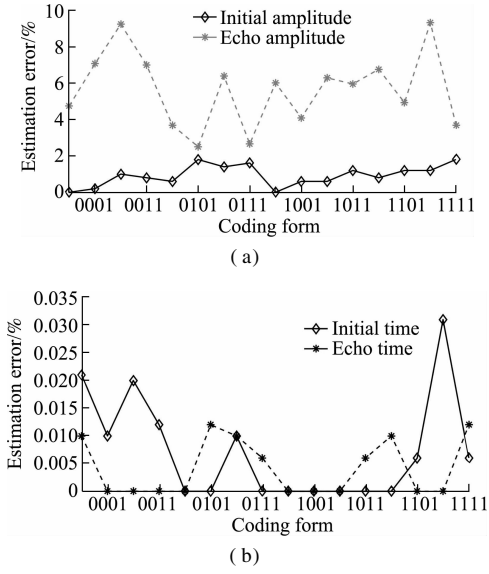

Fig. 9 Parameter estimation error. (a) Amplitude parameter; (b) Time parameter

The converted pulse stream signal could be FRI sparse-sampled, and the amplitude and time of flight of the high-order moment signal could be accurately estimated using the sparse-sampled data. The maximum error of the amplitude was 9.324%. This may be due to the saturation phenomenon when the amplitude of the ultrasonic pulse stream signal exceeds the rated value of analog devices. The maximum error of the time of flight was 0.031%. The FRI sparse sampling frequency was performed at the local maximum innovation rate of the high-order moment pulse stream signal, which was 0.5 MHz. Therefore, the sparse sampling rate was considerably lower than that using the conventional Nyquist sampling method, and the amount of sampling data was considerably reduced.

At the same time, the echo pulse amplitude of the

original coded ultrasonic signal is compared with the echo pulse amplitude of the high-order moment pulse stream. If there are multiple echoes in one detection, the minimum amplitude value is taken, as shown in Fig. 10. When the noise level is constant, extracting the high-order moment pulse stream can improve the SNR by increasing the echo amplitude of the detection signal.

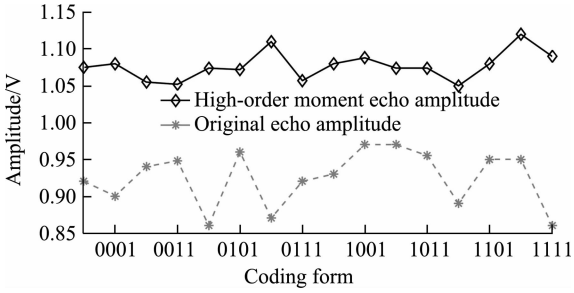

Fig. 10 Comparison of echo amplitudes

5 Conclusions

1) In response to the problem of coded ultrasonic FRI sparse sampling, this study proposed a novel framework by converting the coded ultrasonic echo into a pulse stream to satisfy the requirements of FRI sparse sampling.

2) A circuit has been designed to implement the proposed framework using a high-order-moment-based converting method of twelfth to convert the signal.

3) Experiments have been performed on an aluminum alloy sample using a binary frequency-coded ultrasonic signal with an encoding length of 4. Experimental results show that the coded ultrasonic signal can be FRI sparse-sampled using a high-order-moment-based converting method, and the amplitude and the time of flight of the echo signal can be estimated using the sparse-sampled data with maximum errors of 9.324% and 0.031%, respectively.

4) The sparse sampling rate was 0.5 MHz in the experiments, which is considerably lower than the conventional Nyquist sampling rate of at least 12.8 MHz.

References

[1] Song S P, Qiao M L. Research on ultrasonic testing of plate weld flaw based on NLFM Barker coded excitation method[J]. *Chinese Journal of Scientific Instrument*, 2020, **41**(4): 247 −254. DOI: 10.19650/j.cnki.cjsi.J2006070. (in Chinese)

[2] Hutchins D, Burrascano P, Davis L, et al. Coded waveforms for optimised air-coupled ultrasonic nondestructive evaluation[J]. *Ultrasonics*, 2014, **54**(7): 1745 −1759. DOI: 10.1016/j.ultras.2014.03.007.

[3] Newhouse V L, Cathignol D, Chapelon J Y. Introduction to ultrasonic pseudo-random code systems[J]. *Progress in Medical Imaging*, 1988: 215 − 226. DOI: 10.1007/978-1-4612-3866-9_5.

[4] Polpetta A, Banelli P. Design and performance of Huffman sequences in medical ultrasound coded excitation[J]. *IEEE Transactions on Ultrasonics, Ferroelectrics, and Frequency Control*, 2012, **59**(4): 630 −647. DOI: 10.1109/TUFFC.2012.2242.

[5] Zhao H, L Mo L Y, Gao S K. Barker-coded ultrasound color flow imaging: Theoretical and practical design considerations[J]. *IEEE Transactions on Ultrasonics, Ferroelectrics, and Frequency Control*, 2007, **54**(2): 319 − 331. DOI: 10.1109/TUFFC.2007.246.

[6] Misaridis T, Jensen J A. Use of modulated excitation signals in medical ultrasound. Part Ⅱ: Design and performance for medical imaging applications[J]. *IEEE Transactions on Ultrasonics, Ferroelectrics, and Frequency Control*, 2005, **52**(2): 192 − 207. DOI: 10.1109/TUFFC.2005.1406546.

[7] Misaridis T, Jensen J A. Use of modulated excitation signals in medical ultrasound. Part Ⅱ: Design and performance for medical imaging applications[J]. *IEEE Transactions on Ultrasonics, Ferroelectrics, and Frequency Control*, 2005, **52**(2): 192 − 207. DOI: 10.1109/tuffc.2005.1406546.

[8] Vetterli M, Marziliano P, Blu T. Sampling signals with finite rate of innovation[J]. *IEEE Transactions on Signal Processing*, 2002, **50**(6): 1417 − 1428. DOI: 10.1109/TSP.2002.1003065.

[9] Song S P, Shao Y H. Ultrasonic signal finite rate of innovation sampling method and application based on self-adaptive pulse width[J]. *Chinese Journal of Scientific Instrument*, 2016, **37**(7): 1492 −1499. DOI: 10.19650/j.cnki.cjsi.2016.07.007. (in Chinese)

[10] Fu N, Cao J, Huang G X, et al. Parameter measurement of M-ary PSK signals with finite rate of innovation[J]. *IEEE Transactions on Instrumentation and Measurement*, 2019, **68**(5): 1271 −1283. DOI: 10.1109/TIM.2019.2895438.

[11] Huang G X. *Research on sampling of pulse sequence with finite rate of innovation based on spectral information*[D]. Harbin: Harbin Institute of Technology, 2019. (in Chinese)

[12] Song S P, Jiang Z. Quadrature demodulation based circuit implementation of pulse stream for ultrasonic signal FRI sparse sampling[J]. *Measurement Science and Technology*, 2017, **28**(3): 035005. DOI: 10.1088/1361-6501/28/3/035005.

[13] Berent J, Dragotti P L, Blu T. Sampling piecewise sinusoidal signals with finite rate of innovation methods[J]. *IEEE Transactions on Signal Processing*, 2010, **58**(2): 613 − 625. DOI: 10.1109/TSP.2009.2031717.

[14] Baechler G, Scholefield A, Baboulaz L, et al. Sampling and exact reconstruction of pulses with variable width[J]. *IEEE Transactions on Signal Processing*, 2017, **65**(10): 2629 − 2644. DOI: 10.1109/TSP.2017.2669900.

[15] Tur R, Eldar Y C, Friedman Z. Innovation rate sampling of pulse streams with application to ultrasound imaging[J]. *IEEE Transactions on Signal Process-*

ing, 2011, **59**(4): 1827 - 1842. DOI: 10.1109/TSP.2011.2105480.

[16] Peng C Q. *Research on pipeline ultrasonic testing signal sampling method and application based on finite rate of innovation* [D]. Zhenjiang: Jiangsu University, 2015. (in Chinese)

[17] Shi Y J, Zeng L. Signal reconstruction algorithm of finite rate of innovation with matrix pencil and principal component analysis[J]. *IEICE Transactions on Fundamentals of Electronics, Communications and Computer Sciences*, 2017, **100**(3): 761 - 768. DOI: 10.1587/transfun.e100.a.761.

[18] Edfors O, Sandell M, van de Beek J J, et al. OFDM channel estimation by singular value decomposition [J]. *IEEE Transactions on Communications*, 1998, **46**(7): 931 - 939. DOI: 10.1109/26.701321.

[19] Behar V, Adam D. Parameter optimization of pulse compression in ultrasound imaging systems with coded excitation[J]. *Ultrasonics*, 2004, **42**(10): 1101 - 1109. DOI: 10.1016/j.ultras.2004.02.020.

[20] Hikino O, Belkerdid M A, Malocha D C. Code optimization for direct sequence spread spectrum and SAW-matched filter implementation[J]. *IEEE Transactions on Ultrasonics, Ferroelectrics, and Frequency Control*, 2000, **47**(4): 974 - 983. DOI: 10.1109/58.852081.

[21] Han Q B, Wang P, Zheng H. Modified ultrasonic time-of-flight diffraction testing with Barker code excitation for sizing inclined crack[J]. *Applied Acoustics*, 2018, **140**: 153 - 159. DOI: 10.1016/j.apacoust.2018.05.023.

[22] Li M H, Hayward G. Optimal matched filter design for ultrasonic NDE of coarse grain materials[J]. *AIP Conference Proceedings*, 2016, **1706**(1): 020011. DOI: 10.1063/1.4940457.

[23] Fung A K. A note on the Wiener-Khintchine theorem for autocorrelation [C]//*Proceedings of the IEEE*. IEEE, 1967: 594 - 595. DOI: 10.1109/PROC.1967.5616.

[24] Kulpa J S. Noise radar sidelobe suppression algorithm using mismatched filter approach [J]. *International Journal of Microwave and Wireless Technologies*, 2016, **8**(6): 865 - 869. DOI: 10.1017/s1759078716000945.

[25] Xu L, Zang H, Zhou S. A design method of phase coded waveform and its mismatched filter [J]. *Journal of Xi'an Jiaotong University*, 2016, **50**(4): 54 - 59, 75. DOI: 10.7652/xjtuxb201604009. (in Chinese)

基于有限新息率的二进制频率编码超声信号稀疏采样

宋寿鹏　陈仪倩　胥保文　邱　越

(江苏大学机械工程学院, 镇江 212013)

摘要: 为了实现编码超声信号的稀疏采样,提出了一种基于有限新息率的二进制频率编码超声信号稀疏采样方法. 给出了脉冲类超声信号有限新息率稀疏采样的架构,分析了编码超声与脉冲超声信号的差异,建立了编码超声信号响应数学模型,采用高阶矩方法对编码回波信号进行了时域变换,获取了其脉冲流信号,经过采样核调制后实施等间隔稀疏采样,实现了编码超声的有限新息率稀疏采样. 在此基础上,研制了硬件实现电路,并将该系统在铝合金样品试件上进行了稀疏采样测试,稀疏采样频率降至0.5 MHz(传统奈奎斯特采样频率至少为12.8 MHz),并能从稀疏采样数据中有效估计出回波信号的幅值和时延,最大估计误差分别为9.324%和0.031%. 该研究为利用编码超声信号检测时降低采样速率和减少数据量提供了理论依据和实际应用参考.

关键词: 编码超声信号; 有限新息率; 高阶矩; 稀疏采样; 电路实现

中图分类号: TB551